Physics of the Earth and Planetary Interiors 187 (2011) 188–198

Contents lists available at ScienceDirect

Physics of the Earth and Planetary Interiors

journal homepage: www.elsevier.com/locate/pepi

Multi-protocol palaeointensity determination from middle Brunhes Chron volcanics, Datong Volcanic Province, China

Adrian R. Muxworthy [a,*], Xinlin Ji [b], Victoria Ridley [a,1], Yongxin Pan [b], Liao Chang [c], Lei Wang [b], Andrew P. Roberts [c,2]

[a] Department of Earth Science and Engineering, Imperial College London, South Kensington Campus, London SW7 2AZ, UK
[b] Key Laboratory of Earth's Deep Interior, Institute of Geology and Geophysics, Chinese Academy of Sciences, Beijing 100029, China
[c] School of Ocean and Earth Science, National Oceanography Centre, University of Southampton, Southampton SO14 3ZH, UK

ARTICLE INFO

Article history:
Received 6 August 2010
Received in revised form 7 June 2011
Accepted 8 June 2011
Available online 26 June 2011
Edited by: Keke Zhang

Keywords:
Palaeointensity
Thellier
Wilson
Multi-specimen
Geomagnetic field behaviour

ABSTRACT

A full vector palaeomagnetic analysis of basalts from the Datong Volcanic Province, China, has been carried out to constrain the orientation and magnitude of the geomagnetic field during the mid-Brunhes Chron at approximately 0.41 Ma. Palaeomagnetic directions were determined using thermal demagnetization. Palaeointensity information was determined using a multi-protocol approach: (1) a Thellier-type protocol, (2) the multi-specimen parallel differential partial thermoremanence method, and (3) the Wilson method. The most consistent data set was obtained with the Wilson method, whilst similar average values, with wider data scatter, were obtained with the Thellier method. Higher values were obtained with the multi-specimen method. We suggest that consistency of results from the different protocols, which access different sections of the blocking/unblocking spectra, provide a useful test of the robustness of palaeointensity estimates. A mean virtual dipole moment of $5.4 \pm 0.6 \times 10^{22}$ Am^2 was determined, which agrees well with coeval values from the PINT database and with the higher average palaeointensities for the mid-Brunhes Chron indicated by more continuous sedimentary relative palaeointensity records.

1. Introduction

Records of the ancient absolute geomagnetic field intensity (palaeointensity) through geological time act as a window to geodynamo processes that generate the geomagnetic field. The field is predominantly dipolar, with small deviations due to non-dipole secular variation. Palaeointensity variations can reflect either or both a change in the total field intensity or field morphology. Compared to studies of the direction of the ancient geomagnetic field, global databases contain fewer accurate palaeointensity determinations. A much larger database with more complete temporal and spatial coverage of full-vector geomagnetic determinations is needed to improve our understanding of the geodynamo.

There have been a limited number of studies (Zhu et al., 1986, 1990; Yamamoto et al., 2007) of paleointensities from the Datong Volcanic Province (DVP), China, which is often split into a western section and an eastern section (Fig. 1). Zhu et al. (1986, 1990) determined palaeointensity estimates from lavas ~0.1–0.19 Ma in age from the western DVP using a modified Thellier–Thellier method (Thellier and Thellier, 1959; Coe, 1967). Their estimates are comparable to what might be expected for rocks of that age range from the palaeointensity database (Perrin and Schnepp, 2004) and from the relative palaeointensity record (Horng et al., 2003; Valet et al., 2005; Channell et al., 2008; Roberts, 2008). In a more comprehensive study, Yamamoto et al. (2007) reported palaeointensity estimates from older samples (~0.3–0.4 Ma) from both the western and eastern DVP (Fig. 1). They reported unusually low absolute palaeointensity estimates for middle to early Brunhes Chron volcanics from the eastern DVP. They used three palaeointensity protocols: (1) the Coe-modified Thellier–Thellier method, (2) the microwave protocol (Shaw et al., 1996), and (3) the Shaw method (Shaw, 1974), including the double-heating-technique (DHT) variant (Tsunakawa and Shaw, 1994). All three methods gave similar results, with a virtual dipole moment (VDM) for the eastern DVP lavas of $2.5 \pm 1.0 \times 10^{22}$ Am^2 compared to a database prediction quoted by Yamamoto et al. (2007) of $5.91 \pm 1.74 \times 10^{22}$ Am^2 for rocks of a similar age (Perrin and Schnepp, 2004). Sedimentary relative palaeointensity records from this time interval suggest that the field intensity was generally high (Valet et al., 2005; Roberts, 2008). In addition to these full-vector studies, Liu et al. (1983) measured palaeomagnetic directions from three localities, one of which (Yujiazhai) is in the eastern DVP (Fig. 1).

* Corresponding author. Tel.: +44 20 7594 6442; fax: +44 20 7594 7444.
E-mail address: adrian.muxworthy@imperial.ac.uk (A.R. Muxworthy).
[1] Present address: Department of Earth and Ocean Sciences, University of Liverpool, Liverpool L69 3GP, UK.
[2] Present address: Research School of Earth Sciences, The Australian National University, Canberra, ACT 0200, Australia.

0031-9201/$ - see front matter © 2011 Elsevier B.V. All rights reserved.
doi:10.1016/j.pepi.2011.06.005

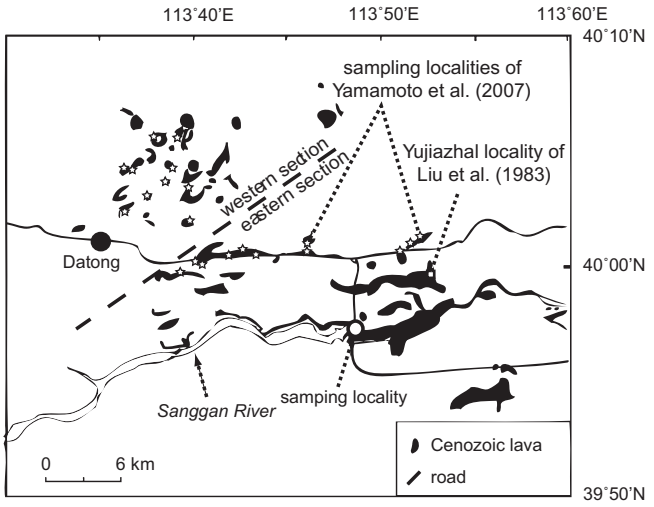

Fig. 1. Map of the western and eastern Datong Volcanic Province, with the sampling localities of this study, Yamamoto et al. (2007) and the Yujiazhai locality of Liu et al. (1983) indicated. The localities sampled by Liu et al. (1983) and Zhu et al. (1986, 1990b) lie outside the area shown on the map.

To investigate the magnetic field behaviour recorded by the eastern DVP volcanics, we report a multi-protocol approach for determining absolute palaeointensities from five lava flows from the eastern DVP. The three protocols employed in this paper are: (1) the Coe-modified Thellier–Thellier method, (2) the multi-specimen parallel differential partial thermoremanent magnetization (pTRM) method, referred to hereafter as the 'multi-specimen' technique (Dekkers and Böhnel, 2006), and (3) the 'Wilson' protocol (Wilson, 1961, 1962; Muxworthy, 2010).

2. Geological setting and sampling

The DVP covers an area of around 50 km^2 (39.5–40.1°N and 113.3–113.9°E) in the Datong basin of the Shanxi Rift system (Fig. 1). Two morphologically distinct volcanic areas exist in the region, with around 20–30 volcanic cones (Xu et al., 2005). Lying southeast of Datong County and trending east-west, the oldest volcanics in the province form the low altitude eastern subgroup which was extruded along now buried basement faults. The younger western subgroup lies to the north of Datong County and trends northeast-southwest having been erupted from volcanic cones that today form high altitude peaks (Xu et al., 2005). The mineralogy of the two subgroups also differs. The eastern DVP lavas are tholeiitic with olivine, plagioclase and augite phenocrysts in a predominantly plagioclase and basaltic glass groundmass, whilst the western alkaline lavas have a groundmass of olivine, augite, glass and plagioclase with phenocrysts of olivine only (Xu et al., 2005). Northeast-southwest-trending normal faults occur throughout the western subgroup. Yamamoto et al. (2007) state that these formed prior to the eruptions because the lava flows have buried and eliminated any grabens that formed at the time.

K–Ar dating by Chen et al. (1992) places the earliest volcanism in the DVP at 0.74 ± 0.23 Ma, whilst the end of the eruptive cycle was at around 0.23 Ma, which calls into question the thermoluminescence ages quoted by Zhu et al. (1986, 1990) of ~0.1–0.19 Ma determined from baked loess. The majority of the Datong volcanics can be dated to the 0.3–0.4 Ma interval (Chen et al., 1992), which suggests that the region was most active during the mid-Brunhes Chron.

For this study, samples were collected in July 2007 from five basaltic flows (CT2-CT6) from the eastern subgroup that crop out in front of a dam in the Sanggan River (Table 1 and Fig. 1). These flows are located further to the south of the eastern section of volcanics examined by Yamamoto et al. (2007). These flows are believed to be temporally discrete because no palaeosols were observed between the flows, which suggest that they were deposited over a relatively short geological time interval. Flow CT2 lies at the base of the exposed unit, and flow CT6 lies at the top of the outcrop. Between 12 and 36 cores (25-mm diameter) were collected from each flow.

Table 1
Localities of the samples and thermomagnetic properties.

Lava	Locality	Rock type	Curie temperature (°C)	Thermomagnetic curve
CT2	39.97403°N, 113.80889°E	Basalt	550–570	Group 1
CT3	39.97403°N, 113.80889°E	Basalt	560–575	Group 1
CT4	39.97403°N, 113.80889°E	Basalt	560–575	Group 2
CT5	39.97403°N, 113.80889°E	Basalt	560–580	Group 1
CT6	39.97403°N, 113.80889°E	Basalt	560–580	Group 2

Attempts to constrain the age of the five studied flows using $^{40}Ar/^{39}Ar$ dating at the Palaeomagnetism and Geochronology Laboratory of the Chinese Academy of Sciences, Beijing, were unsuccessful. The samples have high olivine phenocryst contents, which result in heavy excess argon contamination. Cheng et al. (2006) suggested that the studied basalts are probably from the same flow that is located slightly further upstream and that is dated at 0.41 ± 0.1 Ma (Chen et al., 1992). However, it is possible that the studied flows are from another eruption sequence, which gives a maximum age range for these basalts of 0.23–0.74 Ma.

3. Experimental procedures

We collected standard oriented 25-mm cores in the field. Depending on the palaeomagnetic experiments that were to be conducted, these cores were either cut into 22-mm specimens or were drilled in the laboratory into mini-cores with 10-mm diameter. Palaeomagnetic measurements were conducted in palaeomagnetism laboratories in Beijing and London.

To assess their palaeomagnetic behaviour, the samples were stepwise thermally demagnetized in Beijing. The remanent magnetizations were measured using a 2-G Enterprises cryogenic magnetometer in a magnetically shielded laboratory (ambient field <300 nT). Heating was performed using a Magnetic Measurements TD48 thermal demagnetizer (residual field <10 nT) up to temperatures of 585 or 620 °C with temperature steps of either 40 or 50 °C.

Thellier-type palaeointensity determinations were also made at the palaeomagnetism laboratory in Beijing following the standard double-heating protocol of Coe (1967), with pTRM checks and pTRM-tail checks (Walton, 1984; Riisager and Riisager, 2001). A laboratory field of 40 μT was applied during both heating and cooling cycles for each in-field treatment. Heating steps were made at 100, 150, 200, 250, 300, 350, 400, 450, 500, 520, 530, 540, 550 and 560 °C, with five pTRM checks and three pTRM tail-checks. The samples were cooled slowly over night with water circulation around the heating chamber. To minimize chemical alteration during heating, air was evacuated from the furnace with a primary vacuum pump prior to each heating run, and argon was flushed in and pumped out of the chamber two or three times. Argon gas was circulated through the furnace during the entire heating process. A few milligrams of activated charcoal, a buffer to oxidation/reduction of magnetite, was also introduced into the furnace prior to each run.

Multi-specimen palaeointensity determinations were made using the protocol of Dekkers and Böhnel (2006) with an ASC thermal demagnetization oven and an Agico JR-5A spinner magnetometer at Imperial College London. The basic assumption of the multi-specimen method is that if a sample has a full TRM and if a pTRM is then induced parallel to the TRM, the intensity of the resultant remanence (pTRM and original TRM) will be equal to the original TRM if the laboratory field is equal to the inducing field of the original TRM. If the laboratory field is less than the inducing field, the overall remanence will decrease; if it is greater, the overall remanence will increase. Therefore, simply measuring and plotting the resultant remanence minus the original TRM, for a range of field values, say 10–100 μT, yields the original intensity. Natural samples rarely have a uni-vectorial natural remanent magnetization (NRM) due to viscous overprints. The characteristic remanent magnetization (ChRM) must therefore be isolated before the palaeointensity experiment by a preceding demagnetization treatment; Dekkers and Böhnel (2006) used a thermal pre-treatment of 250 °C. To induce the pTRM parallel to the ChRM, a specially designed sample holder capable of fitting within the oven was used, similar to that used by Michalk et al. (2008). The error in the orientation was <5°. The sample holder only fits 10-mm diameter mini-cores. We applied successively increasing fields in 10 μT steps from 10 to 100 μT. After each remagnetization experiment, the bulk magnetic susceptibility was measured using a Magnon susceptibility meter.

Wilson protocol palaeointensity measurements were conducted at Imperial College London. In the Wilson protocol (Wilson, 1961, 1962), the continuous thermal demagnetization spectrum of the NRM is compared with that for a TRM induced in the same sample in known field. This method is similar to the original method of Folgerhaiter (1899), but instead of measuring at only room temperature, the NRM and TRM are measured at a range of temperatures. No pTRMs are applied in the Wilson protocol, therefore the method is independent of magnetic domain state. However, this method is chemically an 'all or nothing' approach, i.e., unlike Thellier-type protocols, it is not possible to determine palaeointensities from lower temperature sections of the blocking/unblocking spectra before chemical alteration begins. An Orion 3-axis high-temperature, low-field vibrating sample magnetometer (VSM) was used for the Wilson palaeointensity determinations. The instrument is fully automated, which allows rapid data acquisition. Muxworthy (2010) reported a new selection criterion for rejecting altered samples, which was used in this study.

Rock magnetic parameters were assessed by measuring hysteresis properties and back-field demagnetization curves using a Petersen Instruments variable field translation balance (VFTB). Standard hysteresis parameters were determined, i.e., saturation magnetization, M_S, saturation remanence M_{RS}, coercive force, B_C, and coercivity of remanence, B_{CR}. Using the M_{RS}/M_S and B_{CR}/B_C ratios, a 'Day plot' was created (Day et al., 1977). High-temperature stability of the samples was assessed by measuring thermomagnetic curves in air in a field of 1 T using the VFTB.

4. Results

4.1. Rock magnetic results

Our high-temperature thermomagnetic data are categorized into two groups (Fig. 2 and Table 1). Samples in group 1 (Fig. 2a) have a single ferrimagnetic phase with a high Curie temperature (T_C) between 570 and 580 °C, which is indicative of magnetite. Heating and cooling curves are almost reversible, which indicates that minimal thermal alteration has occurred. This behaviour was observed in several samples from flows CT2, CT3 and CT5.

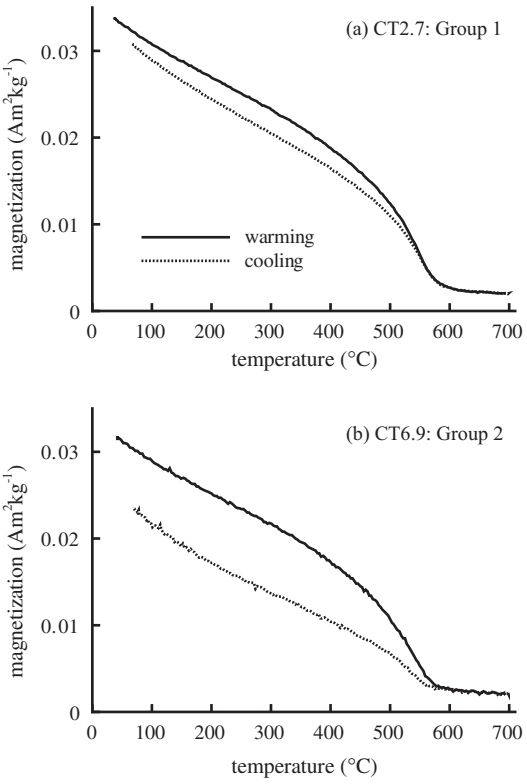

Fig. 2. Representative thermomagnetic curves for: (a) Group 1 (sample CT2.7), and (b) Group 2 (sample CT6.9) samples. A field of 1 T was applied during measurement.

Samples in group 2 (Fig. 2b) have similar heating curves to those from group 1, i.e., a single magnetic phase with high T_C between 570 and 580 °C that is indicative of magnetite; however, the curves are not reversible on cooling. Such thermomagnetic curves, which indicate significant thermal alteration, i.e., oxidation, were observed in samples from flows CT4 and CT6.

Bulk magnetic hysteresis properties for the studied samples are shown in a Day plot (Fig. 3). Data for all five flows plot in the area normally associated with fine-grained pseudo-single domain (PSD)

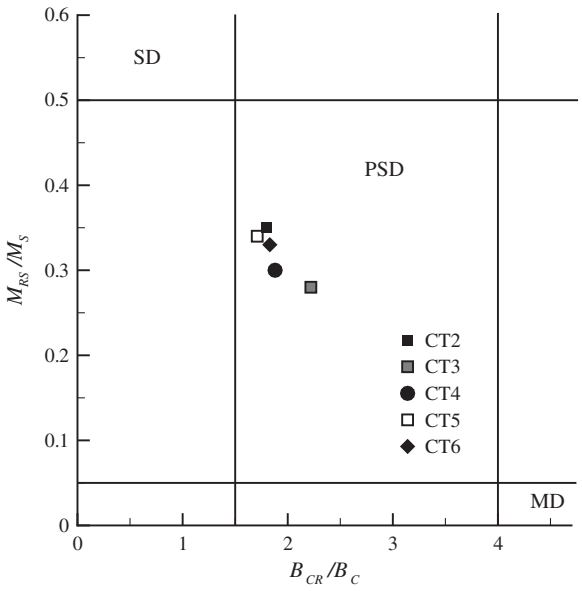

Fig. 3. "Day plot" (Day et al., 1977) of the ratios of the hysteresis parameters M_{RS}/M_S versus B_{CR}/B_C for the five lavas examined in this study. The regions commonly associated with SD, PSD and MD behaviour are labelled.

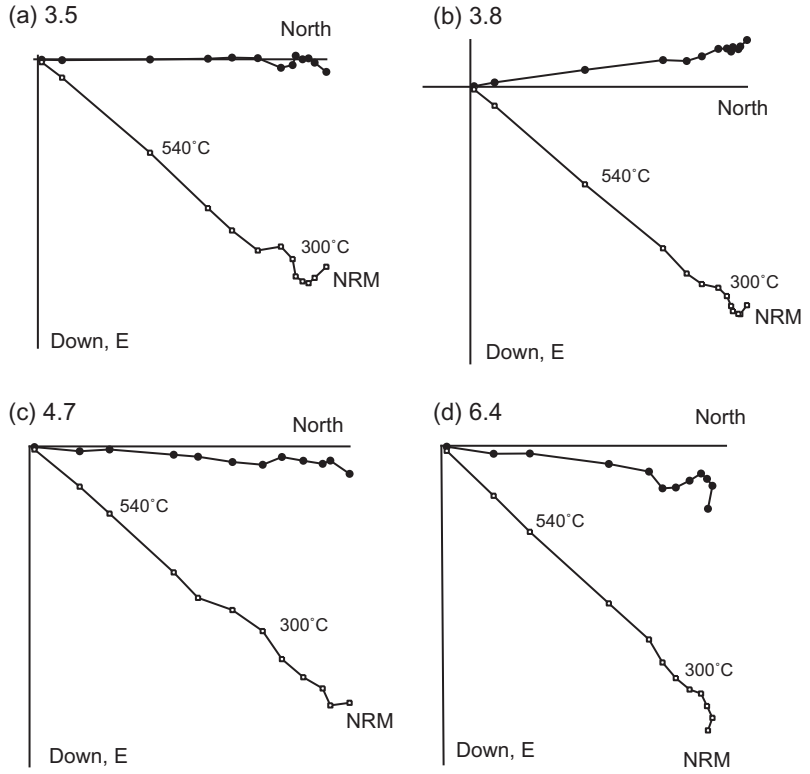

Fig. 4. Orthogonal demagnetization plots for four representative samples. These samples were stepwise thermally demagnetized. Open circles indicate projections onto the vertical plane, whilst closed symbols denote projections onto the horizontal plane.

behaviour, which indicates that the samples are potentially reliable palaeomagnetic recorders.

4.2. Palaeodirectional data

Typical orthogonal demagnetization plots are shown in Fig. 4. Stepwise thermal demagnetization revealed that the samples generally have uni-vectorial magnetizations (Fig. 4); some samples have a weak, probably viscous, magnetization that was removed by at most 250 °C. ChRMs were isolated using principal component analysis. A total of 93 out of 97 samples yielded stable ChRM directions. Lava-mean and group mean directions were calculated using Fisher (1953) statistics (Table 2), and mean flow directions with α_{95} confidence cones are plotted on an equal area stereonet in Fig. 5. The directions of the five flows are tightly clustered with small α_{95} values. They plot slightly to the east of previous directional data from the eastern DVP section (Liu et al., 1983; Yamamoto et al., 2007).

Table 2
Mean palaeomagnetic directions.

Lava	n/N[a]	D[b] (°)	I[b] (°)	k[c]	α_{95}[d] (°)
CT2	10/10	0.3	44.5	405.6	2.2
CT3	13/13	356.3	39.3	161.0	3.1
CT4	29/32	359.3	40.8	840.7	0.9
CT5	22/23	2.2	40.3	562.1	1.3
CT6	19/19	355.8	41.1	84.2	3.7

[a] n/N, the number of samples used to calculate the direction out of the number of samples measured.
[b] Mean declination and inclination of ChRM.
[c] The precision parameter of Fisher (1953).
[d] 95% confidence cone about the mean.

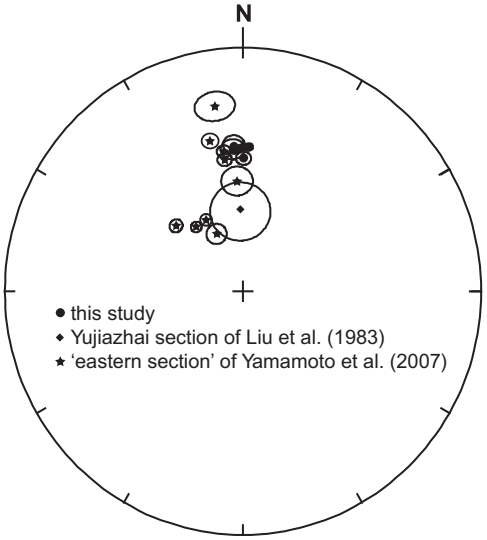

Fig. 5. Equal area stereonet of the ChRM directions for samples in this study, and other results from the 'eastern section' (see Fig. 1), i.e., from Yamamoto et al. (2007) and the Yujiazhai locality of Liu et al. (1983). The 95% confidence cones are plotted.

4.3. Thellier palaeointensity determinations

The Thellier method was used to estimate the palaeointensity from flows CT3 to CT6 (Table 3). The quality of each palaeointensity determination has been evaluated using the statistical parameters developed by Coe et al. (1978). We accepted determinations that satisfied all of the following requirements: (1) at least five consecutive NRM–TRM points used for palaeointensity determination, with NRM fraction $f > 0.3$, and with NRM directions that are

Table 3
Details of accepted Thellier palaeointensity estimates.

Lava	Sample	n[a]	T_{int} (°C)[b]	f[c]	g[d]	q[e]	Estimate (μT)
CT3	3.5	5	520–560	0.56	0.73	6.4	34 ± 2
	3.7	7	450–560	0.75	0.81	6.9	42 ± 4
	3.8	6	450–560	0.77	0.79	7.2	41 ± 4
	3.25	6	500–560	0.66	0.78	6.4	33 ± 3
CT4	4.6	7	200–500	0.62	0.79	6.4	47 ± 4
	4.7	7	200–500	0.63	0.79	8.5	47 ± 3
	4.8	7	200–500	0.63	0.79	11.1	47 ± 2
	4.9	6	200–450	0.45	0.75	5.9	55 ± 3
	4.10	8	200–520	0.71	0.83	7.4	43 ± 3
	4.11	7	200–500	0.60	0.79	7.0	49 ± 3
	4.17	9	200–530	0.73	0.82	8.4	42 ± 3
	4.18	7	400–550	0.6	0.81	5	21 ± 2
	4.19	6	450–550	0.57	0.76	4.9	29 ± 3
	4.32	8	200–520	0.70	0.77	7.5	40 ± 3
	4.33	7	300–530	0.66	0.74	7.7	30 ± 2
CT6	6.5	6	400–540	0.65	0.75	4.9	33 ± 3
	6.11	8	300–540	0.84	0.84	7.3	31 ± 3
	6.12	7	300–530	0.69	0.82	7.3	34 ± 3

[a] Number of points used in the calculation.
[b] The temperature range for which the palaeointensity was determined.
[c] The fraction of NRM used (Coe et al., 1978).
[d] The gap factor (Coe et al., 1978).
[e] Quality factor (Coe et al., 1978).

directed toward the origin of a vector component diagram with maximum angular deviation, MAD <6°; (2) the quality factor q is larger than 2 and the standard-error-of-the-slope/slope (β factor) is <0.1; (3) positive pTRM checks (i.e., within 15% difference normalized to the total TRM), and (4) positive pTRM-tail checks (less than 10% difference normalized to the NRM). Twenty out of ninety samples from three lava flows passed the above quality criteria (Table 3).

Palaeointensity estimates for flow CT3 are derived from the high-temperature segments of Arai plots (Nagata et al., 1963) (Fig. 6a and b). Estimates from flows CT4 and CT6 were selected from a wider temperature range (Fig. 6c, d and f). No successful estimates were made from flow CT2 or CT5 (Fig. 6e). Average palaeointensity values and the 95% confidence intervals (CI_{95}) are listed in Table 4. The standard deviation gives an estimate of the width of the distribution, whereas CI_{95} describes a range within which the mean is likely to lie (Borradaile, 2003; Paterson et al., 2010). CI_{95} is inversely proportional to the square root of the number of samples. The success rate for the palaeointensity determinations is generally low, with samples from flows CT2 and CT5 failing to return an estimate. Samples failed because their magnetic recording capacity altered during the experiment, as indicated by pTRM checks. The average values for all three flows lie close to each other: CT3 (38 ± 5 μT, CI_{95} = 31–45 μT), CT4 (41 ± 10 μT, CI_{95} = 36–46 μT), and CT6 (33 ± 2 μT, CI_{95} = 32–34 μT) (Table 4).

4.4. Multi-specimen palaeointensity determinations

For multi-specimen experiments, it is first necessary to select a temperature for pTRM acquisition that is below the point where chemical alteration is significant and above the temperature at which viscous components persist. Any viscous behaviour is removed by a thermal pre-treatment step, i.e., a thermal-demagnetization step to a temperature less than that at which the pTRM is induced. To determine these temperatures, the NRM of several samples from each flow was stepwise thermally demagnetized at 50 °C steps up to 600 °C (Fig. 4). The NRM of samples from flows CT2 and CT3 sharply demagnetizes near the Curie temperature, whereas for flows CT4, CT5 and CT6 it demagnetizes more gradually (Figs. 4 and 7). A pTRM temperature of 400 °C was initially chosen for all samples because unblocking occurs at relatively high temperatures. Experiments were repeated for flows CT3, CT4 and CT6 with a pTRM temperature of 500 °C. For the other two flows, there was insufficient material for repeat measurements. Thermal pre-treatment was applied at 250 °C because of the high unblocking temperatures, which is 50 °C higher than that used by Dekkers and Böhnel (2006).

Results of multi-specimen palaeointensity experiments are shown for each flow in Fig. 8. Using the standard multi-specimen presentation procedure, we plot the fraction (pTRM–NRM)/NRM (frac pTRM–NRM (%)) versus the applied field (Dekkers and Böhnel, 2006; Michalk et al., 2008; Böhnel et al., 2009). Generally, the data have clear linear trends, with the frac pTRM–NRM percentage increasing with applied field. The data for flow CT2 have the most consistent trend.

The palaeointensity is estimated using the multi-specimen approach where the best-fit line to the trend intersects the field axis. The robustness of these determinations was assessed by determining confidence intervals at 95% for the linear fits (Fig. 8 and Table 4). Previous studies have plotted confidence intervals at 68%, erroneously claiming that this is equivalent to a single standard deviation (Dekkers and Böhnel, 2006; Michalk et al., 2008; Böhnel et al., 2009). Plotting confidence limits at 95% rather than 68% significantly increases the width of the interval. At 95% confidence, some confidence intervals were not defined (ND, Table 4), i.e., the confidence limit does not cross the x-axis, meaning that there is essentially no relationship at this confidence level, and the estimate can be rejected, e.g., both estimates for flow CT3 (Fig. 8b).

Field estimates vary widely from 116 μT (CI_{95} = 100–137 μT) for flow CT2, to 42 μT (CI_{95} = 34–48 μT) for flow CT4 (pTRM induced at 400 °C). Both estimates for flow CT3 failed to yield an upper confidence limit, and a reliable CI_{95} was not determined for flow CT6 (pTRM = 400 °C). Increasing the pTRM induction temperature from 400 to 500 °C increases the gradient, which makes no significant change to the predicted palaeointensity (Table 3 and Fig. 8). However, in the case of flow CT6 this makes it possible to determine a CI_{95}. In the case of flow CT4, confidence limits can be determined for both palaeointensity estimates. In this case, we chose to work with the dataset with the narrower CI_{95}, i.e., the pTRM induced at 400 °C.

As a test for chemical alteration during the experiments, the low-field magnetic susceptibility of the samples was measured after cooling to room temperature. Generally, moderate susceptibility changes were observed, with an average of 3% for flow CT6, and an average of 14% for flow CT5 (Table 4). The susceptibility variation within each flow was relatively uniform.

4.5. Wilson protocol palaeointensity determinations

For each sample, the NRM was continuously thermally demagnetized, a TRM was induced in a known field of 50.3 μT, and the TRM was then continuously thermally demagnetized (Fig. 9). The NRM and TRM demagnetization curves are plotted against each other, and a line is fitted to the data associated with the primary NRM, i.e., above the thermal demagnetization temperature required to begin isolating the identified primary magnetization (Fig. 9). Errors are present in both the NRM and TRM, therefore the line fit is based on minimization of the perpendicular offsets (Bevington and Robinson, 2003). A palaeointensity estimate for each sample is made from the gradient, along with an associated standard error. No samples from flow CT2 were measured because there were insufficient samples to make this possible.

Some samples have highly reversible behaviour (Fig. 9b, f and h), whilst others have strong correlations over sections of the TRM vs. NRM plots (Fig. 9d). Other samples have clear evidence for chemical alteration, in particular samples from flow CT6 (Table

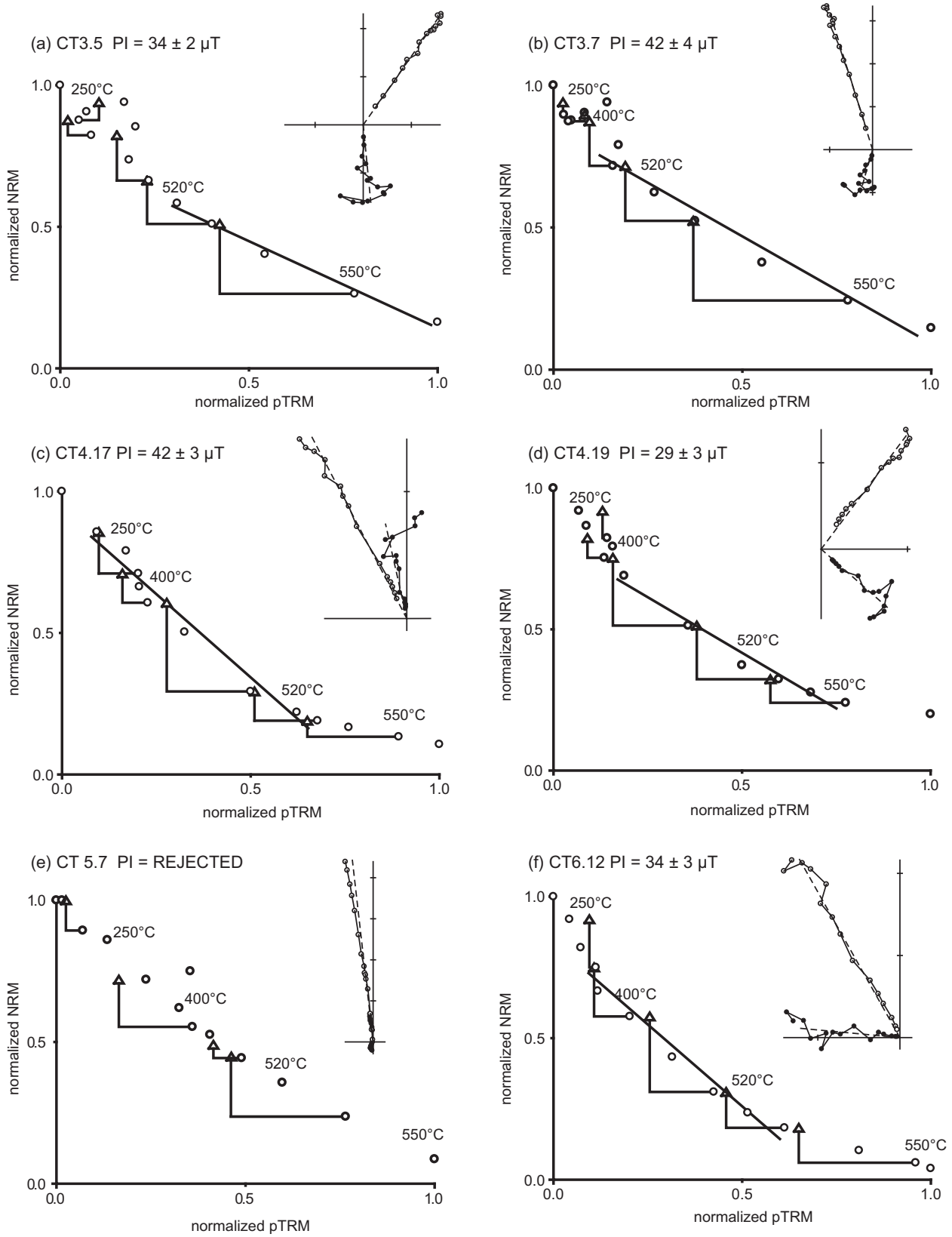

Fig. 6. Representative Arai plots for the three flows with Thellier palaeointensity results: (a) CT3.5, (b) CT3.7, (c) CT4.17, (d) CT4.19, (e) CT5.7 (data rejected), and (f) CT6.12. The inset figure to the upper right of each diagram illustrates the demagnetization behaviour of the specimen on a vector component plot. The palaeointensities were determined using the criteria described in Section 4.2. The palaeointensity (PI) with error is listed on each figure and in Table 3.

5). Examining a suite of historical lavas, Muxworthy (2010) found that when the relative standard error (RSE), i.e., the standard error of the estimate normalized by the applied field, is >0.02 the estimate is more likely to be unreliable due to chemical alteration. Muxworthy (2010) suggested that such Wilson protocol estimates should be rejected. Raw palaeointensity estimates are listed in

Table 4
Palaeointensity estimates for the studied basaltic lavas.

Lava	Palaeointensity estimates (with standard deviation)								
	Thellier			Multi-specimen			Wilson		
	Success ratio[a]	Mean (μT)	CI_{95} (μT)	Estimate (μT)	CI_{95} (μT)	Average susceptibility change (%)	Success ratio[a]	Mean (μT)	CI_{95} (μT)
CT2	0/2	–	–	116[b]	100–137	11	–	–	–
CT3	4/11	38 ± 5	31–45	86[b] 93[c]	48–ND[d] 71–ND[d]	11	15/16	34 ± 5	31–37
CT4	11/36	41 ± 10	36–46	42[b] 47[c]	34–48 32–61	12	4/6	37 ± 11	23–51
CT5	0/22	–	–	47[b]	19–70	14	5/7	38 ± 10	27–49
CT6	3/19	33 ± 2	32–34	61[b] 54[c]	ND[d]–ND[d] 41–69	3	2/10	32 ± 9	16–48

[a] The number of successful samples is the numerator; the denominator is the total number of samples considered.
[b] pTRM inducing temperature was 400 °C.
[c] pTRM inducing temperature was 500 °C.
[d] ND = not defined.

Table 5 and average palaeointensity estimates with 95% confidence intervals are listed in Table 4 for each flow unit. We provide a standard deviation for flow CT6 in Table 4 for consistency, although this value is not statistically correct as it is derived from only two estimates.

5. Discussion

The studied lava flows yielded comparable palaeomagnetic field directions (Table 2 and Fig. 5). Variable palaeointensities were obtained for the three protocols, although none of the techniques returned systematically different estimates (Table 4). Generally, flow CT4 produced the most consistent estimates and the highest values, with almost identical results for the Thellier and multi-specimen protocol (41 ± 10 μT (CI_{95}: 36–46 μT) and 42 μT (CI_{95}: 34–48 μT), respectively), with the Wilson estimate a little lower, but still within error, at 37 ± 11 μT (CI_{95}: 23–51 μT). The Thellier and Wilson protocols give similar results for flow CT3, i.e., 38 ± 5 μT (CI_{95}: 30–44 μT), and 34 ± 5 μT (CI_{95}: 31–37 μT) respectively. In contrast, high values were obtained from the multi-specimen method (>85 μT); however, we reject these determinations because the upper confidence limit could not be defined. No Thellier estimates were obtained from flow CT5, although the other two methods gave similar estimates, but with large confidence intervals (Table 4). Flow CT6 only yielded three Thellier estimates (average 33 ± 2 μT (CI_{95}: 32–34 μT)), out of 19 samples. This low yield may be due to curvature in the Arai plots (Fig. 3) suggesting the presence of MD remanence carriers. With the Wilson method, which is independent of domain state, a palaeointensity estimate of 32 ± 9 μT was obtained for flow CT6 (CI_{95}: 16–48 μT). With the multi-specimen technique, an estimate of 54 μT was obtained (CI_{95}: 41–69 μT) when the pTRM was induced at 500 °C; we rejected the other multi-specimen estimate from flow CT6 because CI_{95} could not be defined. No Thellier estimates and a high multi-specimen estimate were obtained from flow CT2; the multi-specimen estimate has a good linear relationship (Fig. 8a). It is unclear why this anomalously high estimate was obtained from flow CT2. It is possible that the relatively small fraction of remanence (<10%) was activated by heating to just 400 °C. Generally, of the three methods used, the most consistent data sets were obtained with the Wilson method.

5.1. Differences among the three palaeointensity methods

With the exception of flow CT4, the three methods yielded different results. There are probably two main reasons for this: (1) differences in the pTRM temperature range examined by the different techniques, and (2) differences in rejection criteria.

The multi-specimen palaeointensity protocol essentially only examines TRM acquired at low- or intermediate-temperatures, i.e., <400–500 °C in this study, whereas the temperature range over which the other two protocols determine the palaeointensity can be much higher. In particular in this study, five of the Thellier determinations were made at temperature intervals >450 °C, therefore, the Thellier and the multi-specimen protocols assess different sections of the thermal blocking/unblocking spectra. It is possible that chemical weathering preferentially affects one section of this distribution, thereby giving rise to spurious results with one method, but not another, e.g., flows CT2 and CT6 (Table 4). Given the uni-vectorial nature of the remanence (Fig. 4), the Wilson determinations were made over a wider range of temperatures. This makes it less likely for these determinations to be influenced by chemical alteration that may have affected only narrow ranges of the blocking/unblocking spectra. This could explain the more consistent results from the Wilson method (Table 4).

The choice of selection/rejection criteria also affects the resultant palaeointensity values. The rejection rate for our Thellier determinations is higher (78%) than for the other two methods (Wilson = 33% and multi-specimen = 37.5%; Table 4). There are two main reasons for these differences. First, Thellier-type approaches have been refined over decades and many rejection criteria have been developed for these measurements. In contrast, the multi-specimen method is new and has no rejection criteria other than the inability to define confidence intervals, which we introduce in this paper. The Wilson method has not been widely used, and currently has only one rejection criterion (Muxworthy, 2010). Second, the multi-specimen and Wilson protocols are much simpler in design, and it is more difficult to identify possible incorrect palaeointensity estimations. Monitoring of room-temperature susceptibility provides the only fidelity check for the multi-specimen protocol (Table 4). The samples with the largest variations from expected field values, e.g., flow CT2 (Table 2), have similar average variations compared to samples from which more typical palaeointensity results were obtained, e.g., flow CT4. Room-temperature susceptibility therefore appears to be too insensitive to serve as a useful rejection criterion, but there also appears to be no physical or statistical reason for rejecting the anomalously high palaeointensity results for flow CT2 determined using the multi-specimen method.

That flow CT4 yielded consistent results over the different temperature ranges for the three methods suggests that this is the most reliable palaeointensity estimate. We suggest that a multiple palaeointensity protocol approach provides a more useful test of

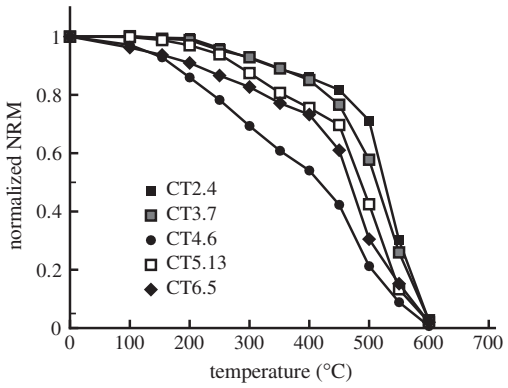

Fig. 7. Stepwise thermal demagnetization curves for representative samples from each flow unit. Such curves were used to select the temperatures for inducing the pTRM in the multi-specimen procedure (Section 4.4 and Fig. 6).

the robustness of palaeointensity results compared to a single protocol approach.

5.2. Palaeosecular variation

Although exact ages for the individual lava flows are unknown, flow CT2 is located at the bottom of the exposure and is the oldest of the studied flows, and flow CT6 is the youngest. The directional data for flows CT2 to CT6 are consistent with each other (Table 2). Palaeointensity data from the three techniques for the five studied flows are scattered, although consistent values were obtained from the Wilson technique for four of the flows, which suggests that little or no secular variation occurred during the eruptive episode. This indicates that the lavas were erupted over a short time interval, as is the case for volcanoes such as Hekla in Iceland, which erupt many times per century, which makes the results in this paper essentially a spot reading of the geomagnetic field. This suggestion is supported by the absence of palaeosols between the flows.

The mean palaeomagnetic directions are compared to published directional data for the 'eastern' DVP section in Fig. 5. Virtual geomagnetic poles (VGPs) are tabulated in Table 6. All of the measurements are spot readings from lavas. It is therefore unlikely that the effects of short-term secular variation have been removed by

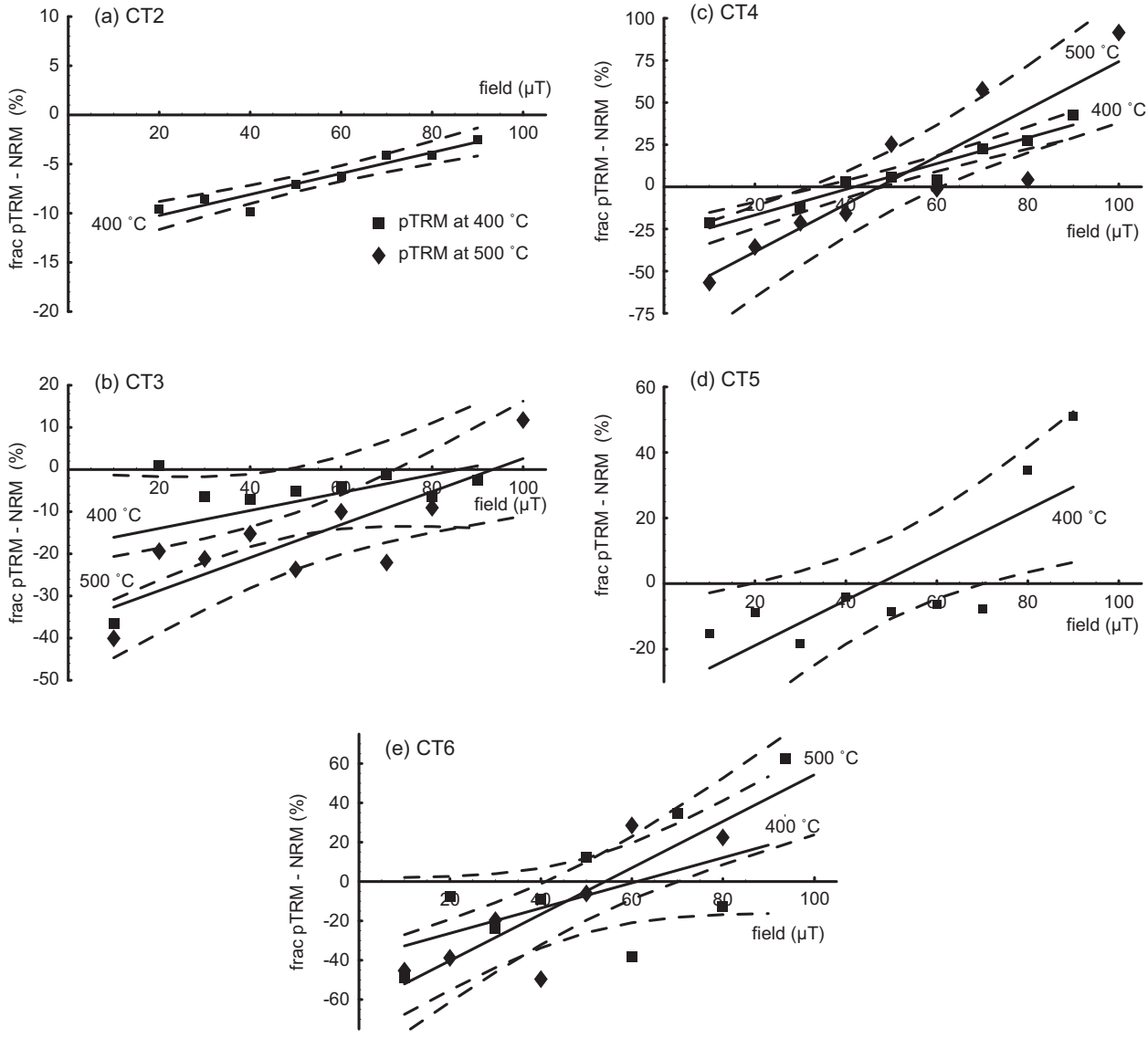

Fig. 8. Plots used to determine the multi-specimen palaeointensity. The percentage of pTRM minus the NRM normalized by the NRM is plotted versus inducing field for sister samples from each flow: (a) CT2, (b) CT3, (c) CT4, (d) CT5, and (e) CT6. Trend lines with 95% confidence limits are plotted. For all flows, the pTRM was induced at 400 °C. For flows CT3, CT4 and CT6, the experiment was repeated with pTRM induced at 500 °C. This generally causes the slope of fitted trend line to become steeper.

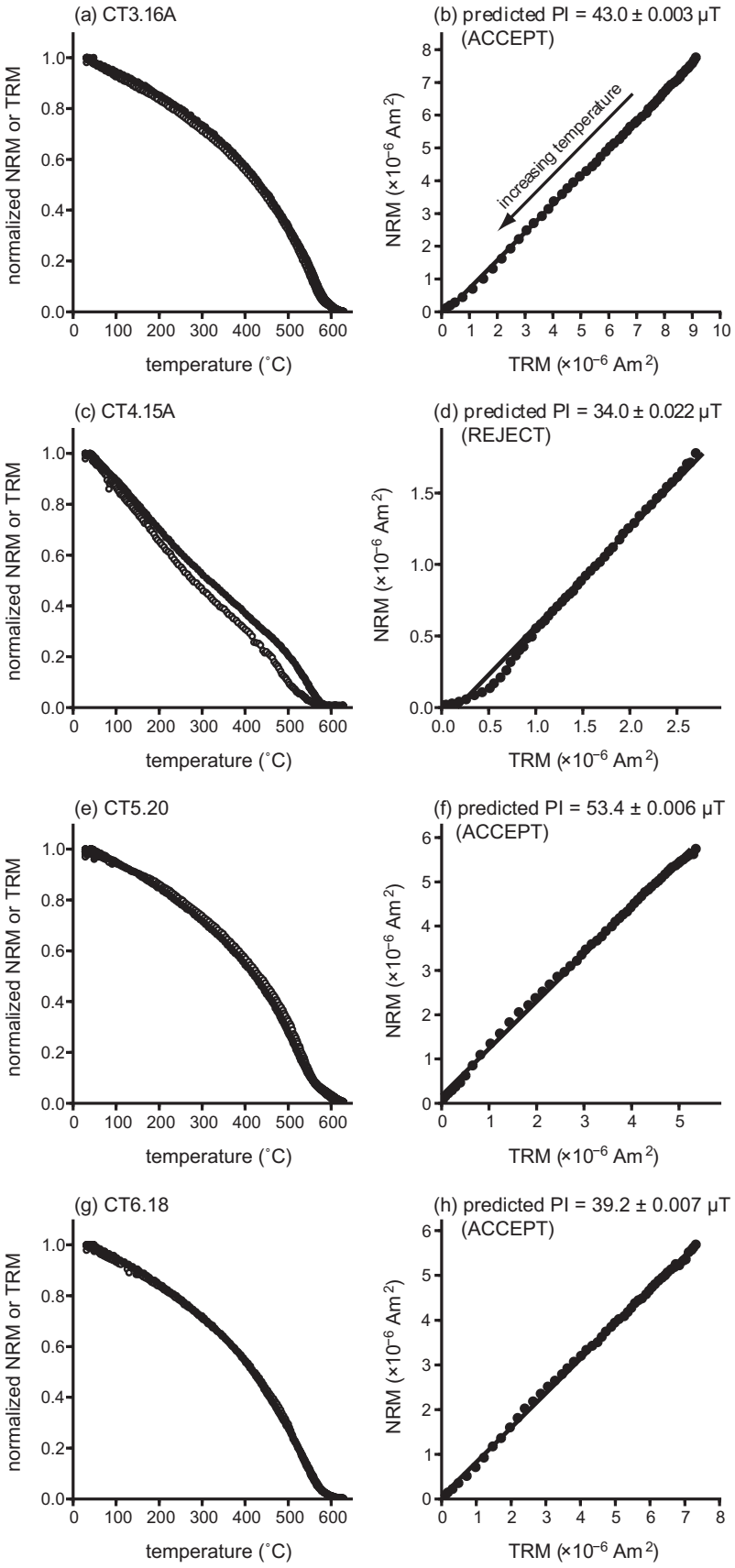

Fig. 9. Data for four representative samples from measurements using the Wilson protocol (CT3.16A, CT4.15A, CT5.20 and CT6.18). The left-hand column contains normalized continuous thermal demagnetization data for the NRM (i.e., TRM). The right-hand column comprises NRM versus TRM plots for the corresponding sample, for which the palaeointensity (PI) estimate is given, with RSE quoted as the error.

Table 5
Details of all the Wilson palaeointensity estimates; rejected data are in italics.

Lava	Sample	Estimate (μT)	RSE
CT3	3.1B	35.95	0.005
	3.16A	42.98	0.004
	3.19	39.10	0.005
	3.20	33.13	0.015
	3.21	39.05	0.005
	3.22A	26.67	0.007
	3.22B	27.17	0.010
	3.23A	25.54	0.008
	3.23B	32.04	0.007
	3.24B	30.36	0.007
	3.25B	32.57	0.008
	3.26B	33.31	0.006
	3.27	39.14	0.004
	3.36	39.62	0.017
	3.37	*49.45*	*0.029*
	3.5	35.01	0.004
CT4	4.2	53.72	0.011
	4.4	*24.84*	*0.023*
	4.5	33.16	0.014
	4.7	34.24	0.014
	4.15	*33.78*	*0.023*
	4.17	27.91	0.013
CT5	5.2	53.41	0.006
	5.3	*27.85*	*0.026*
	5.13	30.40	0.012
	5.18	41.53	0.008
	5.22	*26.37*	*0.051*
	5.24	34.24	0.016
	5.26	30.63	0.007
CT6	*6.1*	*25.07*	*0.029*
	6.2A	*17.63*	*0.050*
	6.2B	*30.08*	*0.024*
	6.8	26.32	0.016
	6.12	*25.31*	*0.024*
	6.14	*20.17*	*0.085*
	6.15	*21.18*	*0.028*
	6.18	39.18	0.006
	6.22	*74.55*	*0.022*
	6.24	*16.02*	*0.048*

averaging. At a 95% confidence limit the mean palaeomagnetic direction and VGP position determined in this study does not align with previous 'eastern' DVP results; however, the VGP position for flow CT6 is indistinguishable from that for flow DX05 (D = 352.0°, I = 41.5°) of Yamamoto et al. (2007) determined using bootstrap statistics at a 95% confidence level (Tauxe et al., 1991). However, the average palaeointensities for these two flows are different: flow CT6 yielded an average from all three techniques of 45 ± 8 μT, compared to two values of 11 ± 2 μT and 12 ± 2 μT determined by Yamamoto et al. (2007) using the LTD-DHT Shaw technique. No results were reported for the standard heating Thellier technique that Yamamoto et al. (2007) employed, and five samples failed to yield a single estimate using the microwave Thellier method. This suggests that the two flows may not have formed at the same time, even though their directions are indistinguishable at the 95% confidence level.

5.3. Average dipole moments during the middle Brunhes Chron

Ignoring the anomalous multi-specimen palaeointensity estimates from flows CT2 and CT3, we have averaged the Thellier, multi-specimen and Wilson estimates (40 ± 4 μT) and determined a VDM of $5.4 \pm 0.6 \times 10^{22}$ Am^2 (Table 6) for the studied DVP sites. We compare our results with those from similar studies in Table 6. Although it is essentially a spot reading, our mean VDM lies close to the expected value determined from the PINT database of $6.7 \pm 2.2 \times 10^{22}$ Am^2 using an age range 0.3–0.5 Ma, and the estimate of Zhu et al. (1990) ($6.21 \pm 0.02 \times 10^{22}$ Am^2) determined for younger rocks, albeit with dating via thermoluminescence. This latter estimate was made from 23 specimens from two flows at slightly different localities. In contrast, the VDM determined in this study is significantly above the VDM estimate of Yamamoto et al. (2007) for eastern DVP volcanics (Table 6), which was determined by pooling all of their data, i.e., LTD-DHT and DHT Shaw, Thellier and microwave data (71 palaeointensity determinations from 9 flows). The average palaeointensity for this data set is 19 ± 8 μT, with a range from 6.8 to 36 μT. Their highest average palaeointensity was obtained from Thellier data (26 ± 13 μT), and the lowest average value was obtained from the microwave method (15 ± 6 μT). These values are significantly lower than those determined in this study.

The most likely reason for the differences in palaeointensity values from different studies of the DVP volcanics is that the lavas provide spot readings of the geomagnetic field and that they were all extruded at different times, as is seen by the different relative positions of their VGPs. Similarly, based on direct dating methods, different ages are claimed in different studies: (1) Zhu et al. (1990) gave an estimated date of 0.1–0.19 Ma, which was determined via thermoluminescence, (2) Yamamoto et al. (2007) judged that their samples were extruded between 0.3 and 0.4 Ma, although this is only a circumstantial estimate, and (3) we estimate the age at 0.41 Ma based on the results of Chen et al. (1992), but we acknowledge that it is potentially as wide as 0.23–0.74 Ma.

5.4. Comparison of middle Brunhes Chron dipole moments with sedimentary records

A further check on the reliability of new results from the DVP is possible via comparison with many detailed relative palaeointensity records that extend through the middle Brunhes Chron (e.g.,

Table 6
Average results for this study and previous DVP studies.

Study		Location		Age (Ma)	VGP		VDM ($\times 10^{22}$ Am^2)
This study		39.97°N	113.81°E	~0.41	73.5°N[b]	297.7°E[b]	5.4 ± 0.6[c]
Liu et al. (1983)	Yujiasai	40.0°N	113.9°E	–	85.2°N	309.0°E	
	Heishan	40.1°N	113.5°E	~0.16[a]	69.0°N	251.0°E	
	Dongshuitou	40.2°N	113.8°E	~0.21[a]	80.0°N	5.2°E	
Zhu et al. (1990)		40.2°N	113.4°E	~0.1–0.19[a]	66.5°N	198.6°E	6.21 ± 0.02
Yamamoto et al. (2007)		Eastern group		~0.30–0.40[d]	76.5°N	7.9°E	2.5 ± 1.0[e]
		Western group					4.7 ± 1.3[e]

[a] Dated using thermoluminescence.
[b] Average of flows CT2 to CT5.
[c] CT6 and multi-specimen data for CT2 and CT3 are excluded.
[d] Date range may be wider than this.
[e] Average of LHT-DHT, Thellier and microwave estimates.

(Horng et al., 2003; Valet et al., 2005; Channell et al., 2008); relative palaeointensity records are more continuous and therefore average the effects of secular variation. Geomagnetic polarity reversals and excursions occur when the field is weak, and in contrast to both the early and late Brunhes Chron when the field was highly variable and where several validated or possible excursions have been recorded, no excursions have been documented for the middle Brunhes Chron (0.3–0.5 Ma) (Laj and Channell, 2007; Roberts, 2008). The higher average palaeointensities from sedimentary palaeointensity records through the middle Brunhes Chron and a lack of excursions are consistent with the higher field determinations obtained in this study and from the PINT database (Perrin and Schnepp, 2004). However, a palaeointensity minimum is still recorded in the middle Brunhes Chron just younger than 0.4 Ma. Given the uncertainty in the age of the flows studied by Yamamoto et al. (2007), it is possible that their younger palaeointensity estimates (spot readings) came from this slightly younger period.

6. Conclusions

Using a multi-protocol approach to estimate the geomagnetic palaeointensity recorded by rocks from the eastern DVP, China, we determined a VDM of $5.4 \pm 0.6 \times 10^{22}$ Am^2. Although this is essentially a spot reading, it compares well with expected values for rocks of this age in the PINT database of $6.7 \pm 2.2 \times 10^{22}$ Am^2 and with generally high relative sedimentary palaeointensities during the mid-Brunhes Chron (e.g., Horng et al., 2003; Valet et al., 2005; Channell et al., 2008). Of the three protocols employed, the most consistent results were obtained with the Wilson method, whilst similar mean values were obtained with the Thellier method but with wider scatter. Higher values were obtained with the multi-specimen protocol; the choice of pTRM inducing temperature is still problematic for the multi-specimen approach and it is suggested that this might be a reason for the variable results. For one well-behaved flow (CT4) similar estimates were obtained with all three methods (Table 4), which suggests that flows that yield consistent results from different protocols (that access different sections of the blocking/unblocking spectra) provide the most reliable palaeointensity estimates.

Our VDM estimates are higher than those of Yamamoto et al. (2007), who determined a VDM of $2.5 \pm 1.0 \times 10^{22}$ Am^2 for eastern DVP rocks using a multi-protocol approach. The VGP positions for the two data sets are significantly different at the 95% level, with the exception of two flows, one from each study, whose directions are indistinguishable at the 95% level. For these two flows, our study yields an intensity estimate that is more than four times stronger, suggesting that they were not extruded at the same time. Our results are closer to those of Zhu et al. (1990) who determined a mean VDM of $6.21 \pm 0.02 \times 10^{22}$ Am^2 using a Thellier-based protocol from rocks with apparently younger ages than those studied here.

Acknowledgement

This work was funded by a joint Royal Society/National Science Foundation of China Joint International Project grant to A.R.M., A.P.R. and Y.P.

References

Bevington, P.R., Robinson, D.K., 2003. Data Reduction and Error Analysis for the Physical Sciences. McGraw-Hill, New York, 328 pp..
Böhnel, H., Dekkers, M., Delgado-Argote, L., 2009. Comparison between the microwave and multispecimen parallel difference pTRM palaeointensity methods. Geophys. J. Int. 177, 383–394.
Borradaile, G., 2003. Statistics of Earth Science Data: Their Distribution in Time, Space and Orientation. Springer Verlag, Heidelberg, 351 pp..
Channell, J.E.T., Hodell, D.A., Xuan, C., Mazaud, A., Stoner, J.S., 2008. Age calibrated relative paleointensity for the last 1.5 Myr at IODP Site U1308 (North Atlantic). Earth Planet. Sci. Lett. 274, 59–71.
Chen, W.J., Li, D.M., Dai, T.M., Pu, Z.P., Liu, R.X., Li, Q., Shun, J.Z., Wang, X., Jager, E., Hurford, A.J., Pfeifer, H.R. (Eds.), 1992. The K–Ar Age and Excess Ar of Quaternary Basalt in Datong. The Age and Geochemistry of Cenozoic Volcanic Rock in China. Seismological Press, Beijing, pp. 81–92.
Cheng, S.-P., Li, C.-Y., Yang, G.-Z., Zhou, S.-W., 2006. Differentiating Pleistocene tectonically driven and climate-related fluvial incision: the Sanggan River, Datong Basin, North China. Geol. Mag. 143, 393–410.
Coe, R.S., 1967. The determination of paleointensities of the Earth's magnetic field with emphasis on mechanisms which could cause non-ideal behavior in Thellier's method. J. Geomag. Geoelect. 19, 157–179.
Coe, R.S., Grommé, S., Mankinen, E.A., 1978. Geomagnetic paleointensities from radiocarbon-dated lava flows on Hawaii and the question of the Pacific nondipole low. J. Geophys. Res. 83, 1740–1756.
Day, R., Fuller, M., Schmidt, V.A., 1977. Hysteresis properties of titanomagnetites: grain-size and compositional dependence. Phys. Earth Planet Int. 13, 260–267.
Dekkers, M.J., Böhnel, H.N., 2006. Reliable absolute palaeointensities independent of magnetic domain state. Earth Planet. Sci. Lett. 248, 508–517.
Fisher, R.A., 1953. Dispersion on a sphere. Proc. Royal Soc. London 217A, 295–305.
Folgerhaiter, G., 1899. Sur les variations séculaires de l'inclinaison magnétique dans l'antiquité. J. Phys. 8, 660–667.
Horng, C.S., Roberts, A.P., Liang, W.T., 2003. A 2.14-Myr astronomically tuned record of relative geomagnetic paleointensity from the western Philippine Sea. J. Geophys. Res. 108 (B1), 2059. doi:10.1029/2001JB001698.
Laj, C., Channell, J.E.T., 2007. Geomagnetic excursions. In: Kono, M. (Ed.), Treatise on Geophysics, first ed. Elsevier Science, Amsterdam, pp. 373–416.
Liu, C., Kazuaki, M., Sadao, S., 1983. Paleomagnetic of some late Cenozoic basalt group from Datong Region, Shanxi Province. Sci. Sinica B 16, 9–16.
Michalk, D., Muxworthy, A.R., Böhnel, H., MacLennan, J., Nowaczyk, N.R., 2008. Evaluation of the multispecimen parallel differential pTRM method: a test on historical lavas from Iceland and Mexico. Geophys. J. Int. 173, 409–420.
Muxworthy, A.R., 2010. Revisiting a domain-state independent method of palaeointensity determination. Phys. Earth Planet Int. 179, 21–31.
Nagata, T., Arai, Y., Momose, K., 1963. Secular variation of the geomagnetic total force during the last 5000 years. J. Geophys. Res. 68, 5277–5281.
Paterson, G.A., Heslop, D., Muxworthy, A.R., 2010. Deriving confidence in paleointensity estimates. Geochem. Geophys. Geosyst. 11, Q07Z18. doi:10.1029/2010gc003071.
Perrin, M., Schnepp, E., 2004. IAGA paleointensity database: distribution and quality of the data set. Phys. Earth Planet Int. 147, 255–267.
Riisager, P., Riisager, J., 2001. Detecting multidomain magnetic grains in Thellier palaeointensity experiments. Phys. Earth Planet Int. 125, 111–117.
Roberts, A.P., 2008. Geomagnetic excursions: knowns and unknowns. Geophys. Res. Lett. 35, L17307. doi:10.1029/2008GL034719.
Shaw, J., 1974. A new method of determining the magnitude of the palaeomagnetic field: application to five historic lavas and five archaeological samples. Geophys. J. Royal Astron. Soc. 39, 133–141.
Shaw, J., Walton, D., Yang, S., Rolph, T.C., Share, J.A., 1996. Microwave archeointensities from Peruvian ceramics. Geophys. J. Int. 124, 241–244.
Tauxe, L., Kylstra, N., Constable, C., 1991. Bootstrap statistics for paleomagnetic data. J. Geophys. Res. 96, 11723–11740.
Thellier, E., Thellier, O., 1959. Sur l'intensité du champ magnétique terrestre dans le passé historique et géologique. Ann. Géophys. 15, 285–376.
Tsunakawa, H., Shaw, J., 1994. The Shaw method of palaeointensity determinations and its application to recent volcanic rocks. Geophys. J. Int. 118, 781–787.
Valet, J.P., Meynadier, L., Guyodo, Y., 2005. Geomagnetic dipole strength and reversal rate over the past two million years. Nature 435, 802–805.
Walton, D., 1984. Re-evaluation of Greek archaeomagnetic intensities. Nature 310, 740–743.
Wilson, R.L., 1961. The thermal demagnetization of natural magnetic moments in rocks. Geophys. J. Int. 5, 45–58.
Wilson, R.L., 1962. An instrument for measuring vector magnetization at high temperatures. Geophys. J. Int. 7, 125–130.
Xu, Y.-G., Ma, J.-L., Frey, F.A., Feigenson, M.D., Liu, J.-F., 2005. Role of lithosphere–asthenosphere interaction in the genesis of Quaternary alkali and tholeiitic basalts from Datong, western North China Craton. Chem. Geol. 224, 247–271.
Yamamoto, Y., Tsunakawa, H., Shaw, J., Kono, M., 2007. Paleomagnetism of the Datong monogenetic volcanoes in China: paleodirection and paleointensity during the middle to early Brunhes Chron. Earth Planets Space 59, 727–746.
Zhu, R.X., Lun, C., Zhu, G., 1986. Determination of geomagnetic palaeointensity of Datong volcanic cluster in the Pleistocene. Kexue Tongbao 31, 369–372.
Zhu, R.X., Liu, C., Zhu, K.K., 1990. Determination of the paleomagnetic field of Datong region and its geological significance. J. Grad. Sch. USTC 7, 72–78.